Nanoscale

PAPER

Cite this: *Nanoscale*, 2022, **14**, 17072

The unrevealed 3D morphological evolution of annealed nanoporous thin films†

Jianqiang Ma,‡[a] Sien Wang,‡[b] Xiao Wan,[a] Dengke Ma,[c] Yue Xiao,[b] Qing Hao*[b] and Nuo Yang*[a]

Received 21st July 2022,
Accepted 23rd October 2022

DOI: 10.1039/d2nr04014j

rsc.li/nanoscale

Nanoporous materials (sub-10 nm in diameter) have potential applications in chips, biosensors, thermoelectrics, desalination and other fields due to their large surface-to-volume ratio. Thermal annealing is a preferred technique to precisely control the ultra-fine nanopore size. Here, the 3D morphological evolution of a membrane with periodic nanopores by thermal annealing is studied. It is found that the evolution is determined by the combination of the membrane thickness, the initial nanopore radius and the periodic length of the porous pattern, rather than the previously suggested ratio between the membrane thickness and pore radius. High-temperature annealing experiments and molecular dynamics simulations are performed to confirm the rationality of the newly proposed model. Energy analysis demonstrates that surface energy minimization is the driving force of the morphological evolution. The local minimum of energy in the new model provides the possibility of thermal stability of nanoporous silicon as a thermoelectric material. This study provides guidance for the mass production of nanoporous membranes with high-temperature annealing.

1. Introduction

Nanoporous materials have significant applications in chips,[1] biosensors,[2] thermoelectrics,[3] desalination,[4] concentrating solar power systems,[5] micro/nano-electronics,[6] data storage[7] *etc*. These applications benefit from the large surface-to-volume ratio and the unique transport and mechanical properties of nanoporous structures. Regarding biosensors, the charged biomolecules driven by an electric field pass through the nanopore one by one.[8] Their highly sensitive detection originates from the structure of the pore, *i.e.*, nanoscale pore sizes not too much larger than that of the detected biomolecule.[9] The diameter of a deoxyribonucleic acid (DNA) chain is about 2 nm, and the size of protein molecules ranges from a few nanometers to tens of nanometers.[10,11] As a selective membrane used for water desalination, pores with a diameter less than 2 nm can retain salt ions while allowing rapid water transport.[12] The expansion of the pore size will result in an order of magnitude reduction in selectivity.[4] The good performance of the thermoelectric material is also determined by periodic nanopores with a small neck width between the adjacent nanopores.[13–15]

Various fabrication techniques have been studied by researchers to achieve nanopores with sub-10 nm diameters and nanometer precision.[16–20] Among them, a focused electron beam in a transmission electron microscope (TEM)[19] and a focused ion beam (FIB)[18] are two popular nanopore fabrication methods. Sub-10 nm or even atomic-sized pores can be fabricated across ultra-thin membranes or atomic-thick materials.[21] For mass production, traditional dry etching or wet etching is often employed for nanopore fabrication but the required dimension is hard to achieve.[22] For these nanopore-fabrication techniques, the smallest nanopore diameter d is restricted by the film thickness t, with an aspect ratio $t/d < 3$.[23] To achieve a high aspect ratio, heated nanoparticles as etching agents can be used.[24]

Another approach to overcome this difficulty is to reduce the pore size by post-annealing, during which the membrane is softened and deformed to a lower surface free energy.[25] With its fine resolution and direct visual feedback during the process, annealing under a TEM would reduce the pore to any size, with single-nanometer precision.[19] Direct thermal heating results in the shrinking of silicon dioxide nanopores with a similar mechanism.[16] Many pores can be processed in one step while keeping the surrounding surface composition the same.[26,27] And high-temperature annealing is a common

[a]*School of Energy and Power Engineering, Huazhong University of Science and Technology, Wuhan 430074, China. E-mail: nuo@hust.edu.cn*
[b]*Department of Aerospace and Mechanical Engineering, University of Arizona, Tucson, AZ, 85721-0119, USA. E-mail: qinghao@arizona.edu*
[c]*NNU-SULI Thermal Energy Research Center (NSTER) & Center for Quantum Transport and Thermal Energy Science (CQTES), School of Physics and Technology, Nanjing Normal University, Nanjing 210023, China*

†Electronic supplementary information (ESI) available. See DOI: https://doi.org/10.1039/d2nr04014j

‡These authors contributed equally to this work.

technique for the preparation of nanostructures, which has an important effect on the surface morphological and optical properties.[28–30]

The surface tension of the softened silicon causes the morphological change, shrinking or expansion, of nanopores. Based on the experimental observation for the same silicon membrane, the small pores would shrink and eventually disappear, while the large pores expand.[16,19] These different morphological changes are determined by the radius–thickness ratio according to a classical model considering the surface energy variation with pore-size changes. The structure will deform to a structure with a lower surface free energy, manifested as the shrinking or expansion of nanopores. Similar physics of shrinking or expansion has also been observed in gold sheets with nanopores[31] and in mercury films of micrometer-scale.[32]

However, fewer works reveal the fundamental physics at the atomic scale. As an atomistic modeling method, molecular dynamics (MD) simulations can provide valuable insight into the physics of the formation and variation of nanoparticles and nanopores.[33–37] For instance, realistic silica nanopores are created for MD simulations by distinguishing nonbridging or bridging oxygens and adding the hydroxyl groups.[38] In addition, the melting of silicon nanoparticles is in good agreement with the experimental observation, such as the size dependence of melting point obtained from simulations.[39,40]

In this work, the deformation processes of nanoporous silicon membranes are investigated through both simulations and experiments. The initial parameters of the nanoporous membrane include the pore radius, membrane thickness and the periodic length of the nanopore array. The results obtained in the experiments and MD simulations are normalized to a mathematical model to explain the morphological changes. Besides, the simulated energy distribution and mean atomic potential energy prove a decrease in surface free energy under thermal annealing treatment. Furthermore, the temperature dependence of nanopore deformation is also investigated.

2. Results and discussion

2.1. Theoretical model of evolution

The schematic figure of a periodic nanoporous silicon membrane is shown in Fig. 1A, where r, h, and p are the nanopore radius, membrane thickness and periodic length, respectively. The simulation cell before relaxation is depicted in Fig. 1B, where silicon atoms have a diamond crystal configuration. After relaxation at elevated temperatures, the atoms at boundaries were re-organized to minimize the surface free energy.

The characteristic length of the theory is the size below which the surface tension is dominant compared with the gravity. The assumption of the proposed theoretical model is that the size of the structure is smaller than the characteristic length.

When the periodic length is much larger than the pore radius, the film thickness is almost unchanged during the

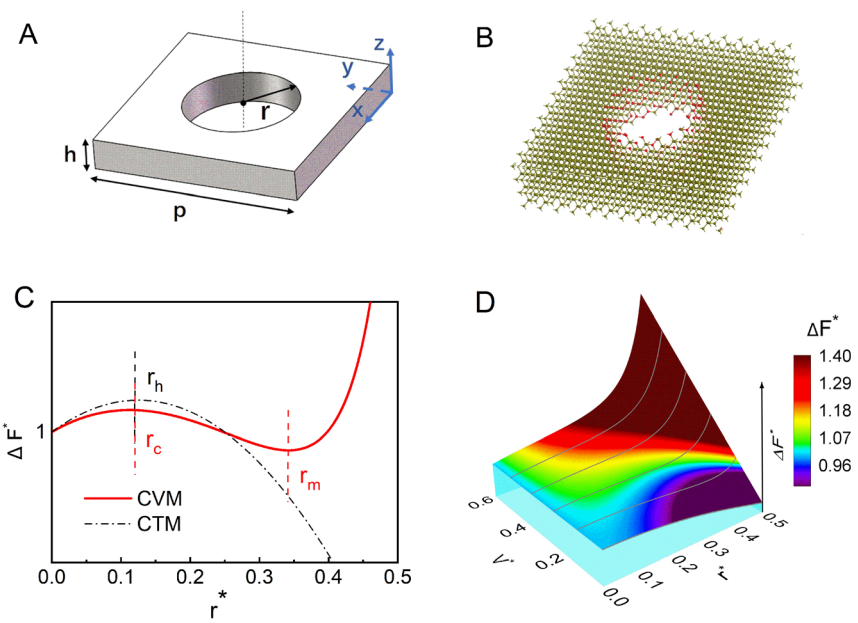

Fig. 1 (A) Schematic of the nanoporous silicon membrane. (B) Schematic views of the simulation cell of the crystalline silicon structure with round pores. The red atoms represent the surface atoms located on the sidewall of the nanopore. (C) The change of surface free energy (ΔF^*) with the normalized radius (r^*) for the CVM, in comparison with the CTM. The dimensionless parameters are: $\Delta F^* = \Delta F/(2p^2\gamma)$, $V^* = V/p^3$, $h^* = h/p$, $r^* = r/p$. It can be seen that for the CVM, the surface free energy reaches the peak at r_c and reaches the trough at r_m, while for the CTM, the curve only has maximum r_h. (D) Comparison of the volume dependences obtained from the CVM. The color change from red to purple means that ΔF^* is decreasing, and parallel gray curves represent V^* as different constants.

expansion or shrinking process. Storm *et al.* described the change in the free energy as[19]

$$\Delta F = \gamma \Delta A = 2\gamma(p^2 - \pi r^2 + \pi r h), \quad (1a)$$

where γ is the surface tension of the viscous fluid and ΔA is the change in the total surface area. It can be written in a normalized form using $\Delta F^* = \Delta F/2p^2\gamma$, $r^* = r/p$, $h^* = h/p$:

$$\Delta F* = 1 - \pi r*^2 + \pi r * h* \quad (1b)$$

The functional relationship between ΔF^* and r^* in eqn (1b) is shown as the constant thickness model (CTM) in Fig. 1C. When h^* is constant, it can be inferred that nanopores with r smaller (larger) than $h/2$ will shrink (expand) to reach a lower surface free energy.

Instead of isolated pores, an array of nanopores is often used in applications, such as phononic crystals.[15,33,41–43] Due to the narrow neck width between the adjacent nanopores, the assumption in eqn (1b) becomes invalid. The change in the local film thickness around pores, caused by the mass flow, should be further addressed. As two extreme cases, amorphous silicon and crystalline silicon have <3% divergence in the density,[44] so the volume of the membrane can be approximated as constant during high-temperature annealing. The model with a constant volume can thus be proposed as:

$$\Delta F = \gamma \Delta A = 2\gamma\left(p^2 - \pi r^2 + \pi r \frac{V}{p^2 - \pi r^2}\right), \quad (2a)$$

or

$$\Delta F^* = 1 - \pi r^{*2} + \pi r^* \frac{V^*}{1 - \pi r^{*2}}, \quad (2b)$$

where V is the volume of one period and the dimensionless $V^* = V/p^3$. Here h in eqn (1a) is replaced with an averaged thickness associated with the volume, and eqn (2b) is the normalized form of eqn (2a). When the periodic length is much larger than the radius, eqn (2b) can be simplified to eqn (1b).

Based on eqn (2b), the relationship between ΔF^* and r^* is shown as the constant volume model (CVM) in Fig. 1C, with a V^* of 0.2. For both models, nanopores with r^* smaller than a critical value (r_c for the CVM and r_h for the CTM) will shrink to lower the surface free energy (ΔF^*). The contrast lies in the ΔF^* trend beyond the critical value. Here the CTM predicts continuously expanded nanopores for an initial r^* larger than r_h. In contrast, the CVM predicts a stable r_m as the local minimum of ΔF^*. For nanopores with an initial $r^* > r_m$, they should shrink to r_m eventually.

In Fig. 1D, the three-dimensional contour of ΔF^* more intuitively reflects the V^* dependence of nanopore deformations. The critical values r_c and r_m for the CVM are correlated with the V^* of the membrane. This can be obtained by the V^*-dependent r_c and r_m given in Fig. S1 in ESI I,† which shows that $|r_m - r_c|$ decreases as the V^* increases. It can also be seen from Fig. S1† that for $V^* > 0.27$, the local minimum r_m disappears and the ΔF^* increases monotonously with the increase of r^*. In this situation, nanopores with different initial radii will shrink and eventually disappear under the drive of the viscous force. For $V^* < 0.27$, nanopores with $r^* < r_c$ will shrink, whereas nanopores with $r_m > r^* > r_c$ will expand to r_m as the final status, as discussed earlier.

2.2. Observation of morphological evolution

Experimentally, nanoporous silicon membranes were prepared, with the film thickness of either 70 nm or 220 nm. Using a commercial silicon-on-insulator (SOI) wafer, the membranes were released from the substrate by etching away the buried oxide layer with diluted hydrofluoric acid. Nanopores, with their radii of ~50 nm to 120 nm, were then drilled using a FIB using Ga ions. After the nanopore drilling, the nanoporous silicon membranes were annealed at high temperatures to tune the nanopore diameter. The temperature was ramped up to the setpoint (annealing temperature) at a rate of 5 K min^{-1} to minimize the thermal stress inside the membrane and then maintained at the annealing temperature for 180 minutes. For suspended membranes, the impact of the substrate on their deformation[45] can be excluded to ascertain that the deformation was entirely driven by the minimization of the surface energy. Details are provided in ESI II.†

Fig. 2A and C show the SEM images of two nanoporous membranes (NM-1 and NM-2) before annealing. These nanopores were drilled in membranes of 220 nm/70 nm thickness using a FIB. The cross-sectional plan of a nanopore is trapezoidal, which is typical for such drilling processes.[46] Fig. 2B (NM-1) and Fig. 2D (NM-2) display the corresponding SEM images after annealing at 1323/1223 K for 180 minutes, under nitrogen protection.

The controlled shrinking and expansion of nanopores in this experiment are inconsistent with previous observations. For isolated nanopores, existing experiments always agree with the CTM, which is not the case for periodic nanopores addressed in this work. In Fig. 2A, the radius of nanopores in NM-1 (111 nm) is about half its thickness (220 nm) and the structure should be stable based on the CTM. However, nanopores in NM-1 shrank in annealing experiments (Fig. 2B). For NM-2 (Fig. 2C and D), the CTM predicts expanded nanopores but stable nanoporous structures were found in experiments.

2.3. Morphological evolution in simulations

The evolution processes of nanopores were tracked in MD simulations (Fig. 3A). In simulations, the equilibrium MD method was used to predict the structural deformation[47,48] (details in ESI III†). These structures are first equilibrated under the canonical ensemble (NVT) at 300 K for 0.15 ns, followed by relaxation under the microcanonical ensemble (NVE) for 0.25 ns. The Langevin heat reservoir is used to heat up the structures from 0.4 ns. The applied temperature needs to be appropriate, which should not only provide sufficient fluidity to soften the pore edges but also avoid fast collapse of the structure. As shown in the inset of Fig. 3A, the applied temperature is 1500 K on the membrane with a V^* of 0.21 and 1700 K on thicker membranes. More explanations are given in ESI IV.†

For the two structures with smaller volumes (V^* of 0.21 and 0.28), the nanopores expand with the annealing time and

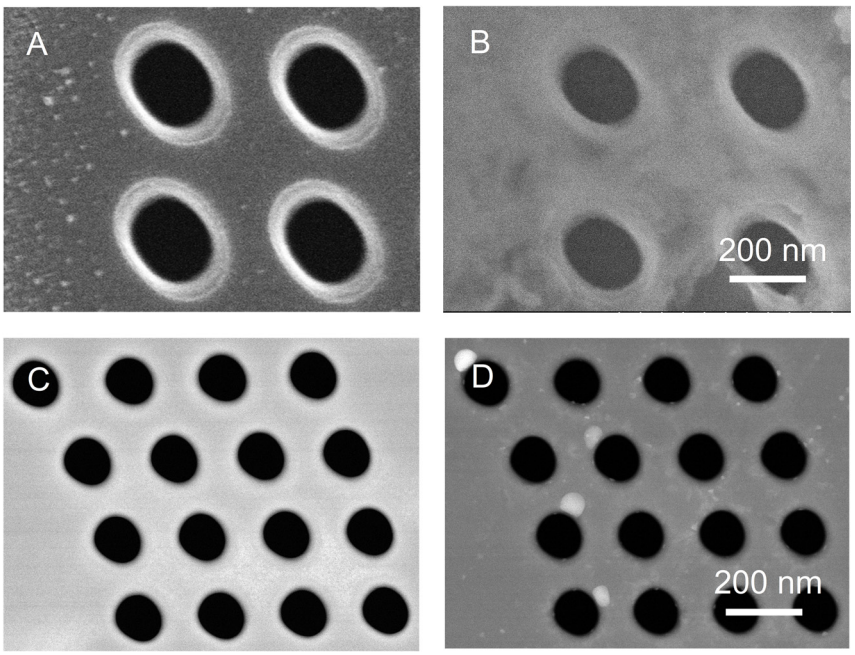

Fig. 2 SEM images (top view) of two nanoporous membranes, NM-1 and NM-2. NM-1: (A) before and (B) after the high-temperature annealing. NM-2: (C) before and (D) after the high-temperature annealing. For NM-1 (NM-2), the pitch p is 400 nm (200 nm), the nanopore radius r is 111 nm (52 nm), and the film thickness h is 220 nm (70 nm).

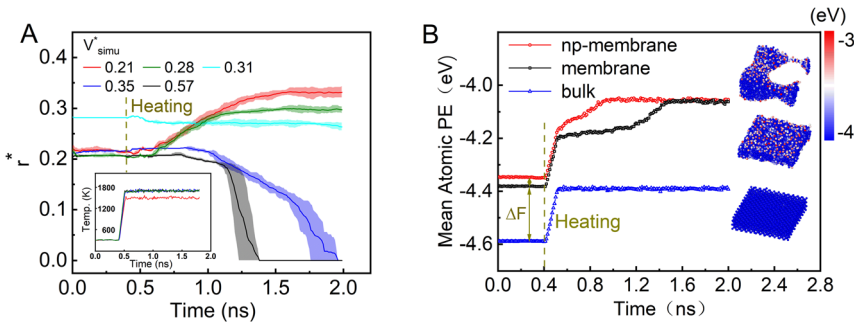

Fig. 3 (A) The size evolution of nanopores based on different V^* values in the simulation. The temperature evolutions of several structures are illustrated in the inset. (B) Mean atomic PE evolution with time. In comparison, the black curve represents a solid membrane whose thickness is the same as that of a nanoporous membrane with V^* = 0.21. The blue curve represents bulk silicon. The inset is the PE distribution of the three configurations.

gradually saturate. For structures with larger volumes (V^* of 0.35 and 0.57), the nanopores shrank until they disappeared, whereas the nanopores remained stable with a V^* of 0.31. More detailed discussions will be given in the next section.

The mean atomic potential energy (PE) in evolution processes was also recorded to further explain the deformations of nanopores. Here the difference between the mean atomic PE of the silicon membrane and bulk silicon could represent the surface free energy. And amorphous silicon has a higher PE than crystalline silicon because of the destruction of the atom distribution with the lowest energy. As shown in Fig. 3B, the change in the mean atomic PE of three structures comes from the surface deformation and phase transition. The disappearance of the initial PE difference between the silicon membrane with (red line) and without (black line) nanopores indicates that the surface free energy of the nanoporous membrane decreases after the deformation because there was almost no deformation for the solid membrane.

From the PE distribution (the inset of Fig. 3B), it can be seen that the PE of surface atoms is higher than that of internal atoms after the silicon crystal melts. As shown in the inset of Fig. 3B, the color evolution from blue to red represents an increase in the atomic PE. For the above two membrane structures, the visible atoms are mostly surface atoms, except for the z-direction atoms due to the periodic boundary. And for the bottom bulk structure, all atoms are internal atoms because of periodic boundaries in three directions. Surface atoms have a higher PE than internal atoms because they have

weaker bond networks and fewer neighboring atoms. As a result, surface atoms with an additional PE spontaneously tend to move away from pore edges under the viscous force, which reduces the surface free energy. The inset also shows that the nanopores cannot keep a perfect cylindrical shape after high-temperature annealing. Instead, a curved nanopore sidewall can be found, with its smallest diameter at the half film thickness location. This can be explained by considering the local forces generated by the surface tension (more explanations are given in Fig. S3 in ESI V†).

2.4. Analysis of evolution

As mentioned earlier, the evolution of nanopores was observed by both experiments and simulations. The observations in experiments (Fig. 4A) and MD simulations (Fig. 4B) were compared with the predictions by the CVM.

In experiments (Fig. 4A), for membranes with the V^* of 0.33 and 0.42, nanopores shrank. It is consistent with the prediction of the CVM in Fig. 1D that nanopores in membranes with $V^* > 0.27$ always tend to shrink. And for $V^* < 0.27$ (0.11 and 0.14 in Fig. 4A), nanopores with an initial radius greater than the critical radius r_c expanded to the vicinity of r_m, the local minimum of ΔF^*, instead of expanding indefinitely. It can also be concluded that the CVM is more suitable than the CTM for an array of nanopores. For a V^* of 0.28, only slight expansion was observed, which can be attributed to the weak ΔF^* dependence on r^* around the initial point.

In simulations (Fig. 4B), the initial and final radii of the nanopores in different structures are obtained from the simulation results in Fig. 3A. The conclusion drawn from Fig. 4B is similar to the experimental results. The critical V^* for nanopores to remain stable is 0.31, slightly more than 0.27. As a boundary, nanopores expand for a smaller V^* and shrink for a larger V^*.

In Fig. 4A and B, the experimental and simulated results both agree well with the theoretical predictions. Combined with the theoretical curves in Fig. 4A and B, the final size of nanopore expansion in an array should be around r_m, as a critical nanopore size for the thermal stability of nanoporous membranes. The deformation rates of nanopores in Fig. 3A follow the $d\Delta F^*/dr^*$ slope in Fig. 4B when the deformation process is completely driven by the surface free energy. More discussions for the failure of the CTM can be found in ESI VII.†

Here, the sizes of both the simulation cell (sub-10 nm) and the measured samples (sub-100 nm) are much smaller than the characteristic length of softened silicon (~100 μm, derived in ESI VIII†). Therefore, both the simulations and the measured results can be used to validate the theoretical constant volume model.

2.5. Temperature effect on evolution

The temperature dependence of deformations is also investigated. As shown in Fig. 5A, the nanopores with the same initial structure at different annealing temperatures exhibit different expansion rates and final nanopore sizes. It can be seen that there is very little change in the size of nanopores at 1300 K due to the limited fluidity of softened Si. At an increased annealing temperature, surface atoms are more likely to migrate under the drive of the surface tension. At a temperature of 1500 K, the r^* increases to the lowest energy point r_m for the given porous structure. When the annealing temperature increases to 1700 K, the pore shape becomes non-circular and the connecting area between the pores disappears.

It can also be observed that the deformation rate of the structure can be largely affected by the annealing temperature. When the temperature reaches 1700 K, the expansion or shrinking rate is too fast and it is difficult to control the pore area accurately. At the same time, the membrane may be broken during the nanopore deformation process due to the large atomic kinetic energy and high stress. The sample breakage caused by a high stress at high temperatures could also be found in the experiment (shown in Fig. 5B). Nevertheless, the expansion/shrinking trend of nanopores is independent of the temperature.

To better evaluate the influence of temperature on the deformation rate, both mean-squared displacement (MSD)[49] and radial distribution function (RDF)[50] are recorded in the simulation. MSD characterizes the diffusion behavior of all

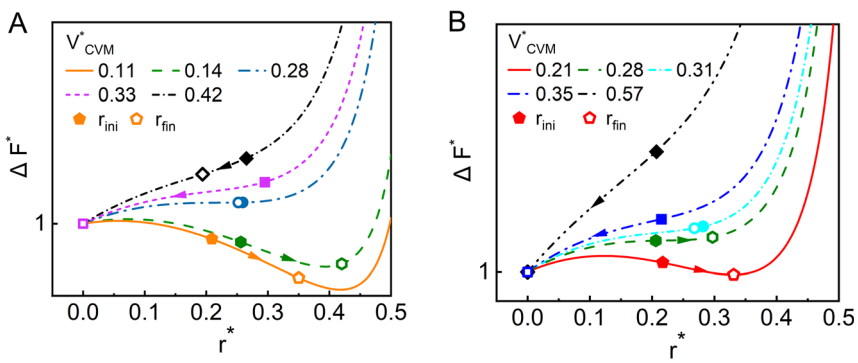

Fig. 4 The normalized surface free energy (ΔF^*) *versus* the normalized radius (r^*). (A) Comparison between the experimental and theoretical results. The solid symbols represent the initial structure, and the hollow symbols represent the evolved structure after the high-temperature annealing. Curves for different V^* values in the CVM are plotted. (B) Comparison between the simulation and theoretical results. Again, solid and hollow symbols represent the nanopore sizes before and after high-temperature annealing, respectively. The lines are theoretical calculations based on eqn (2b) and the solid symbols are measurements (A) or simulations (B). The original data are shown in Table S2 in ESI VI.†

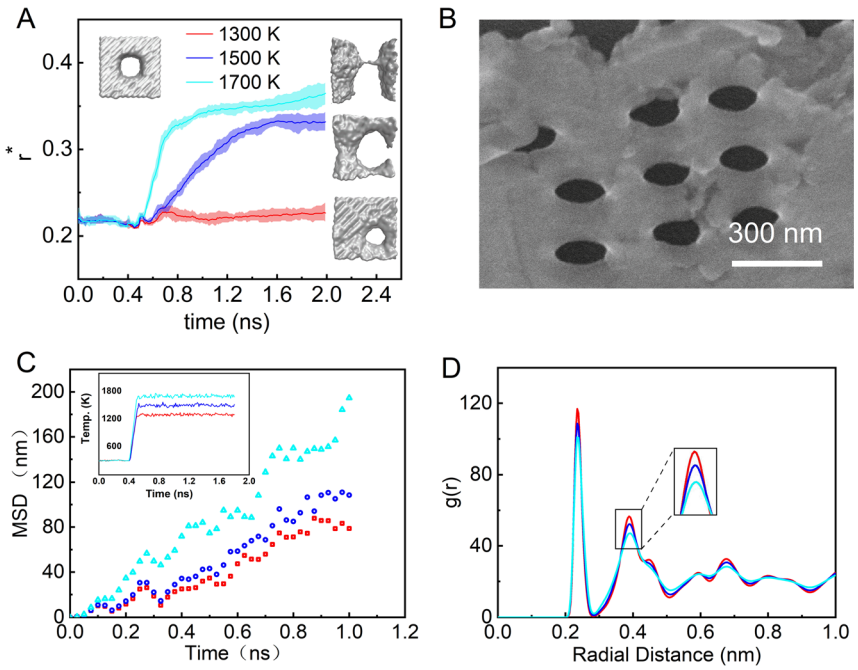

Fig. 5 (A) Nanopore evolution at different temperatures, with the V^* fixed at 0.21. The temperature evolutions are illustrated in the inset in (C). (B) SEM image of a damaged nanoporous membrane treated at 1323 K. (C) Mean-squared displacement of all atoms at different temperatures. (D) Radial distribution functions of annealed nanoporous membranes at 0.05 ns. Curves of different colors represent the state of the same nanoporous membrane at different annealing temperatures.

atoms over a period of time. As shown in Fig. 5C, when the annealing temperature is higher, the particles have a longer displacement distance and correspondingly a larger diffusion constant. RDF represents the degree of disorder caused by the melting of the initial crystal structure. As shown in Fig. 5D, the peak of RDF for a structure with a higher annealing temperature is more gradual, which means a high degree of disorder for the lattice. It can be concluded that a higher temperature could accelerate the inward propagation speed of surface melting and amorphization.[39]

For thermoelectrics, the thermoelectric figure of merit (ZT) of nanostructured Si usually monotonously increases with the temperature.[51,52] In this case, the thermal stability of nanoporous Si can largely restrict its applications for high-temperature energy harvesting. As shown in Fig. 5A, even if the edge of the nanopore is softened at 1500 K, the nanopore may still maintain a stable pore size r_m with the lowest surface energy, which can also be proved by the experimental results in Fig. 4A. Future studies may be extended to general nanoporous thin films for the structure stability at high temperatures when other factors such as oxidation can be eliminated.

3. Conclusion

In summary, the evolution of nanopores in silicon membranes during high-temperature annealing is systematically studied by both experiments and MD simulations. Compared with the previous assumption of a constant membrane thickness to predict the final size of the nanopore, the proposed constant volume model is proven to be more accurate for periodic nanoporous structures. The major difference is the prediction of a stable nanopore radius as the local minimum of surface free energy for some cases, which may be used to maintain nanofeatures at a high temperature.

In MD analysis, a higher potential energy is found for surface atoms due to the dangling chemical bonds. The mass flow driven by the surface tension is to reduce the surface free energy to achieve a more stable structure. The expansion/shrinking dynamics mainly depends on the initial configuration of the nanoporous pattern. The annealing temperature has a strong influence on the deformation rate of nanopores but does not affect the pore expansion/shrinking trend. In practice, an excessive annealing temperature would cause the membrane to break due to large strains in the morphological evolution process.

This work reveals the mechanism of morphological evolution of nanopores and provides guidance for the mass production of nanoporous membranes.

Conflicts of interest

There are no conflicts of interest to declare.

Acknowledgements

N. Y. is sponsored by the National Key Research and Development Project of China No. 2018YFE0127800, and

Fundamental Research Funds for the Central Universities No. 2019kfyRCPY045. Q. H. acknowledges the support from the Craig M. Berge Dean's Fellowship. FIB and TEM analyses were performed at the Kuiper Materials Imaging and Characterization Facility and Q. H. gratefully acknowledges NSF (grant #1531243) for funding of the instrumentation in the Kuiper Materials Imaging and Characterization Facility at the University of Arizona. We are grateful to Shichen Deng, Ke Xu and Lina Yang for useful discussions. N. Y. thanks the National Supercomputing Center in Tianjin (NSCC-TJ) and the China Scientific Computing Grid (ScGrid) for providing assistance in computations.

References

1 M. Brinker, G. Dittrich, C. Richert, P. Lakner, T. Krekeler, T. F. Keller, N. Huber and P. Huber, Giant electrochemical actuation in a nanoporous silicon-polypyrrole hybrid material, *Sci. Adv.*, 2020, **6**(40), eaba1483.

2 K. Chen, I. Jou, N. Ermann, M. Muthukumar, U. F. Keyser and N. A. W. Bell, Dynamics of driven polymer transport through a nanopore, *Nat. Phys.*, 2021, **17**, 1043–1049.

3 L. Yang, N. Yang and B. Li, Extreme Low Thermal Conductivity in Nanoscale 3D Si Phononic Crystal with Spherical Pores, *Nano Lett.*, 2014, **14**(4), 1734–1738.

4 S. P. Surwade, S. N. Smirnov, I. V. Vlassiouk, R. R. Unocic, G. M. Veith, S. Dai and S. M. Mahurin, Water desalination using nanoporous single-layer graphene, *Nat. Nanotechnol.*, 2015, **10**(5), 459–464.

5 C. Wang, W. Cheng, P. Ma, R. Xia and X. Ling, High performance Al–AlN solar spectrally selective coatings with a self-assembled nanostructure AlN anti-reflective layer, *J. Mater. Chem. A*, 2017, **5**(6), 2852–2860.

6 J.-K. Hong, H.-S. Yang, M.-H. Jo, H.-H. Park and S.-Y. Choi, Preparation and characterization of porous silica xerogel film for low dielectric application, *Thin Solid Films*, 1997, **308–309**, 495–500.

7 G. Wang, Y. Yang, J. Lee, V. Abramova, H. Fei, G. Ruan, E. L. Thomas and J. M. Tour, Nanoporous Silicon Oxide Memory, *Nano Lett.*, 2014, **14**(8), 4694–4699.

8 M. Wanunu, W. Morrison, Y. Rabin, A. Y. Grosberg and A. Meller, Electrostatic focusing of unlabelled DNA into nanoscale pores using a salt gradient, *Nat. Nanotechnol.*, 2010, **5**(2), 160–165.

9 M.-H. Lee, A. Kumar, K.-B. Park, S.-Y. Cho, H.-M. Kim, M.-C. Lim, Y.-R. Kim and K.-B. Kim, A Low-Noise Solid-State Nanopore Platform Based on a Highly Insulating Substrate, *Sci. Rep.*, 2014, **4**(1), 7448.

10 A. Singer, S. Rapireddy, D. H. Ly and A. Meller, Electronic Barcoding of a Viral Gene at the Single-Molecule Level, *Nano Lett.*, 2012, **12**(3), 1722–1728.

11 L. J. Steinbock, S. Krishnan, R. D. Bulushev, S. Borgeaud, M. Blokesch, L. Feletti and A. Radenovic, Probing the size of proteins with glass nanopores, *Nanoscale*, 2014, **6**(23), 14380–14387.

12 D. Cohen-Tanugi and J. C. Grossman, Water Desalination across Nanoporous Graphene, *Nano Lett.*, 2012, **12**(7), 3602–3608.

13 S. Alaie, D. F. Goettler, M. Su, Z. C. Leseman, C. M. Reinke and I. El-Kady, Thermal transport in phononic crystals and the observation of coherent phonon scattering at room temperature, *Nat. Commun.*, 2015, **6**(1), 7228.

14 Y. Liao, T. Shiga, M. Kashiwagi and J. Shiomi, Akhiezer mechanism limits coherent heat conduction in phononic crystals, *Phys. Rev. B*, 2018, **98**(13), 134307.

15 Y. Xiao, Q. Chen, D. Ma, N. Yang and Q. Hao, Phonon Transport within Periodic Porous Structures—From Classical Phonon Size Effects to Wave Effects, *ES Mater. Manuf.*, 2019, **5**, 2–18.

16 W. Asghar, A. Ilyas, J. A. Billo and S. M. Iqbal, Shrinking of Solid-state Nanopores by Direct Thermal Heating, *Nanoscale Res. Lett.*, 2011, **6**, 1–6.

17 C. Jian, D. Tao, L. Zewen and S. Haizhi, Controllable shrinking of silicon oxide nanopores by high temperature annealing, in 2017 China Semiconductor Technology International Conference (CSTIC), 12–13 March 2017, IEEE, Piscataway, NJ, USA, 2017, p. 3.

18 J. Li, D. Stein, C. McMullan, D. Branton, M. J. Aziz and J. A. Golovchenko, Ion-beam sculpting at nanometre length scales, *Nature*, 2001, **412**(6843), 166–169.

19 A. J. Storm, J. H. Chen, X. S. Ling, H. W. Zandbergen and C. Dekker, Fabrication of solid-state nanopores with single-nanometre precision, *Nat. Mater.*, 2003, **2**(8), 537–540.

20 A. J. Storm, J. H. Chen, X. S. Ling, H. W. Zandbergen and C. Dekker, Electron-beam-induced deformations of SiO_2 nanostructures, *J. Appl. Phys.*, 2005, **98**(1), 014307.

21 C. J. Russo and J. A. Golovchenko, Atom-by-atom nucleation and growth of graphene nanopores, *Proc. Natl. Acad. Sci. U. S. A.*, 2012, **109**(16), 5953.

22 S. R. Park, H. Peng and X. S. Ling, Fabrication of Nanopores in Silicon Chips Using Feedback Chemical Etching, *Small*, 2007, **3**(1), 116–119.

23 A. M. Marconnet, M. Asheghi and K. E. Goodson, From the Casimir Limit to Phononic Crystals: 20 Years of Phonon Transport Studies Using Silicon-on-Insulator Technology, *J. Heat Transfer*, 2013, **135**(6), 061601.

24 N. R. Kadasala, M. Saei, G. J. Cheng and A. Wei, Dry Etching with Nanoparticles: Formation of High Aspect-Ratio Pores and Channels Using Magnetic Gold Nanoclusters, *Adv. Mater.*, 2018, **30**(3), 1703091.

25 Y. S. Nagornov, Thermodynamics of annealing of nanoporous silicon, *Tech. Phys. Lett.*, 2015, **41**(6), 532–536.

26 C. J. Lo, T. Aref and A. Bezryadin, Fabrication of symmetric sub-5 nm nanopores using focused ion and electron beams, *Nanotechnology*, 2006, **17**(13), 3264–3267.

27 D. Tao, C. Jian, L. Mengwei and L. Zewen, Shrinking of silicon nanopore arrays by direct dry-oxygen oxidation, in 2013 IEEE 13th International Conference on Nanotechnology (IEEE-NANO), 5–8 Aug. 2013, IEEE, Piscataway, NJ, USA, 2013, pp. 586–589.

28 N. A. M. Noor, S. K. Mohamad, S. S. Hamil, M. Devarajan and M. Z. Pakhuruddin, Effects of annealing temperature towards surface morphological and optical properties of black silicon fabricated by silver-assisted chemical etching, *Mater. Sci. Semicond. Process.*, 2019, **91**, 167–173.

29 A. M. Alwan and M. Q. Zayer, The Effects of Rapid Thermal Annealing on Photoluminescence Properties of Nanostructures Silicon, *Journal of Al-Nahrain University*, 2012, **15**(2), 88–92.

30 L. Jacobsohn, D. Cooke, B. Bennett, R. Muenchausen and M. Nastasi, Effects of thermal annealing and ageing on porous silicon photoluminescence, *Philos. Mag.*, 2005, **85**(23), 2611–2620.

31 M. Lanxner, C. Bauer and R. Scholz, Evolution of hole size and shape in {100},{110} and {111} monocrystalline thin films of gold, *Thin Solid Films*, 1987, **150**(2–3), 323–335.

32 G. Taylor and D. Michael, On making holes in a sheet of fluid, *J. Fluid Mech.*, 1973, **58**(4), 625–639.

33 D. Ma, H. Ding, H. Meng, L. Feng, Y. Wu, J. Shiomi and N. Yang, Nano-cross-junction effect on phonon transport in silicon nanowire cages, *Phys. Rev. B*, 2016, **94**(16), 165434.

34 L. Yang, N. Yang and B. Li, Thermoelectric properties of nanoscale three dimensional Si phononic crystals, *Int. J. Heat Mass Transfer*, 2016, **99**, 102–106.

35 H. Wang, S. Hu, K. Takahashi, X. Zhang, H. Takamatsu and J. Chen, Experimental study of thermal rectification in suspended monolayer graphene, *Nat. Commun.*, 2017, **8**(1), 1–8.

36 S. Hu, Z. Zhang, P. Jiang, J. Chen, S. Volz, M. Nomura and B. Li, Randomness-induced phonon localization in graphene heat conduction, *J. Phys. Chem. Lett.*, 2018, **9**(14), 3959–3968.

37 S. Hu, Z. Zhang, P. Jiang, W. Ren, C. Yu, J. Shiomi and J. Chen, Disorder limits the coherent phonon transport in two-dimensional phononic crystal structures, *Nanoscale*, 2019, **11**(24), 11839–11846.

38 J. Geske and M. Vogel, Creating realistic silica nanopores for molecular dynamics simulations, *Mol. Simul.*, 2016, **43**(1), 13–18.

39 K. C. Fang and C. I. Weng, An investigation into the melting of silicon nanoclusters using molecular dynamics simulations, *Nanotechnology*, 2005, **16**(2), 250–256.

40 I. V. Talyzin, M. V. Samsonov, V. M. Samsonov, M. Y. Pushkar and V. V. Dronnikov, Size Dependence of the Melting Point of Silicon Nanoparticles: Molecular Dynamics and Thermodynamic Simulation, *Semiconductors*, 2019, **53**(7), 947–953.

41 C. Zhou, N. Tambo, E. M. Ashley, Y. Liao, J. Shiomi, K. Takahashi, G. S. W. Craig and P. F. Nealey, Enhanced Reduction of Thermal Conductivity in Amorphous Silicon Nitride-Containing Phononic Crystals Fabricated Using Directed Self-Assembly of Block Copolymers, *ACS Nano*, 2020, **14**(6), 6980–6989.

42 R. Anufriev, J. Maire and M. Nomura, Reduction of thermal conductivity by surface scattering of phonons in periodic silicon nanostructures, *Phys. Rev. B*, 2016, **93**(4), 045411.

43 J. Maire, R. Anufriev, R. Yanagisawa, A. Ramiere, S. Volz and M. Nomura, Heat conduction tuning by wave nature of phonons, *Sci. Adv.*, 2017, **3**(8), e1700027.

44 J. S. Custer, M. O. Thompson, D. Jacobson, J. Poate, S. Roorda, W. Sinke and F. Spaepen, Density of amorphous Si, *Appl. Phys. Lett.*, 1994, **64**(4), 437–439.

45 Q. Hao, Y. Xiao and F. J. Medina, Annealing Studies of Nanoporous Si Thin Films Fabricated by Dry Etch, *ES Mater. Manuf.*, 2019, **6**, 24–27.

46 Q. Hao, D. Xu, H. Zhao, Y. Xiao and F. J. Medina, Thermal studies of nanoporous Si films with pitches on the order of 100 nm—Comparison between different pore-drilling techniques, *Sci. Rep.*, 2018, **8**(1), 1–9.

47 L. de Sousa Oliveira and N. Neophytou, Large-scale molecular dynamics investigation of geometrical features in nanoporous Si, *Phys. Rev. B*, 2019, **100**(3), 035409.

48 A. J. McGaughey and M. Kaviany, Phonon transport in molecular dynamics simulations: formulation and thermal conductivity prediction, *Adv. Heat Transfer*, 2006, **39**, 169–255.

49 J.-P. Hansen and I. R. McDonald, *Theory of simple liquids*, Elsevier, 1990.

50 J. G. Kirkwood and E. M. Boggs, The radial distribution function in liquids, *J. Chem. Phys.*, 1942, **10**(6), 394–402.

51 Q. Hao, D. Xu, N. Lu and H. Zhao, High-throughput Z T predictions of nanoporous bulk materials as next-generation thermoelectric materials: A material genome approach, *Phys. Rev. B*, 2016, **93**(20), 205206.

52 Q. Hao, G. Zhu, G. Joshi, X. Wang, A. Minnich, Z. Ren and G. Chen, Theoretical studies on the thermoelectric figure of merit of nanograined bulk silicon, *Appl. Phys. Lett.*, 2010, **97**(6), 063109.

Supplementary Materials for

The Unrevealed 3D Morphological Evolution for Annealed Nanoporous Thin Films

Jianqiang Ma[1#], Sien Wang[2#], Xiao Wan[1], Dengke Ma[3], Yue Xiao[2], Qing Hao[2*], Nuo Yang[1*]

1. School of Energy and Power Engineering, Huazhong University of Science and Technology, Wuhan 430074, China.

2. Department of Aerospace and Mechanical Engineering, University of Arizona, Tucson, AZ, 85721-0119, USA

3. NNU-SULI Thermal Energy Research Center (NSTER) & Center for Quantum Transport and Thermal Energy Science (CQTES), School of Physics and Technology, Nanjing Normal University, Nanjing 210023, China.

# J.M. and S.W. contributed equally to this work.

* Corresponding email: qinghao@arizona.edu (Q.H.), nuo@hust.edu.cn (N.Y.)

I. Volume dependence of critical radius r_c and r_m

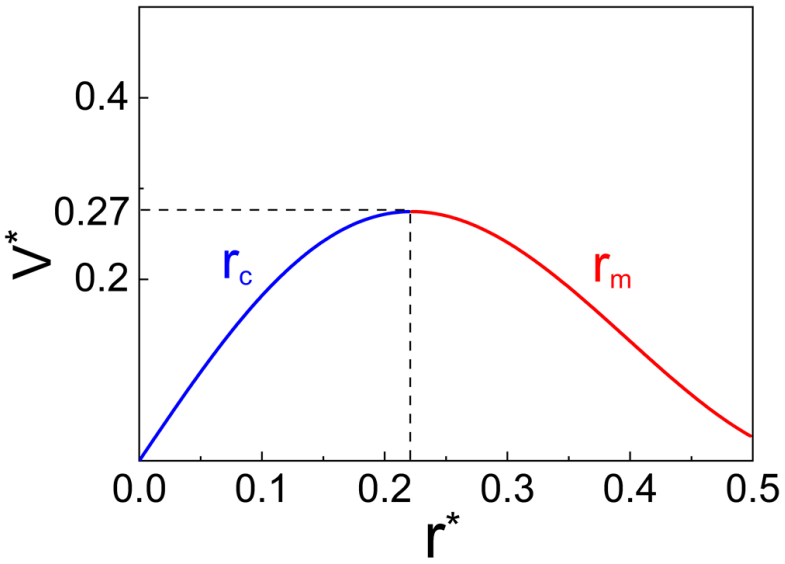

Figure S1 The normalized volume V^* dependence of critical radius r_c and r_m .

Set the derivative of surface free energy change ΔF^* with respect to the radius r^* in Eq. (2b) to zero. The resulting critical radius expressions contain V^*, which can be formulated as follows:

$$V^* = \frac{2\pi^2 r^{*5} - 4\pi r^{*3} + 2r^*}{1 + \pi r^{*2}} \qquad (S1)$$

And the $V^* - r^*$ functional relationship is plotted in Figure S1. It can be concluded that when the V^* is greater than 0.27, the critical radius r_c and r_m disappears, and the ΔF^* in Figure 1C increases monotonically with the increase of the r^*.

II. Sample preparation and high-temperature annealing experimental process

The 70-nm-thick Si thin film used in the annealing study came from the device layer of a silicon-on-insulator (SOI) substrate. The film was released from the substrate by etching away the buried oxide layer in diluted hydrofluoric acid. Nanopores of different sizes were drilled with a Ga^+ Focused Ion Beam (FIB). The beam voltage and current for the milling process were chosen to be 30 keV and 7.7 pA.

The annealing was carried out in a furnace with nitrogen protection throughout

the entire process. A higher flow rate was used to purge the annealing chamber before processing and then maintained at 10 scfm. The temperature was ramped up to the setpoint (annealing temperature) at a rate of 5 K/min to minimize the thermal stress inside the film and then maintained at the annealing temperature for 2-3 hours. Then the temperature was ramped down to the ambient at the same rate.

Electron microscopy studies were carried out before and after the annealing to study the morphology of the nanopore. The STEM/TEM images were taken with the Hitachi HF-5000 TEM. The SEM images were taken with the FEI Helios NanoLab 660.

III. EMD simulation process and parameter settings

The equilibrium molecular dynamics (EMD) method is used to simulate structural deformation [1, 2]. All EMD simulations in this work are performed by the large-scale atomic/molecular massively parallel simulator (LAMMPS) packages [3]. The interactions between atoms are described by a modified Tersoff potential, which reproduces a wide range of properties of silicon such as surface energies and reconstructions, melting temperature [4]. The free and periodic boundary conditions are applied in the z-axis and other two directions, respectively. And the velocity Verlet algorithm is employed to integrate equations of motion [5]. Here 0.2 fs and 3.2 Å are chosen as time step and cutoff distance for the Tersoff potential, respectively.

As shown in Figure 1B, one of the simulation cells is built by 12×12×3 silicon single crystal cells, which means that the periodic length l is 6.52 nm and the thickness h is 1.63 nm. The atomic arrangement is in line with the regular diamond structure with a bond length of 0.235 nm. In the LAMMPS approach, the size of the simulation box is 6.52 ×6.52 × 41.62 nm^3, which is the same with silicon supercell in x and y directions and much larger in the z-direction. The nanoporous silicon structure was firstly equilibrated at 300K for 0.15 ns in the canonical ensemble (*NVT*) and then in the microcanonical ensemble (*NVE*) for 0.15 ns. Afterward, the Langevin thermostat is used to increase the system temperature from 300 K to 1300 K and higher temperature.

Then Langevin thermostat runs for 1.5 ns to record atomic coordinates and calculate the pore area.

Table S1 Parameter settings in MD simulation.

Method	Equilibrium MD				
Potential	Tersoff				
Boundary conditions	x y z: periodic, periodic, periodic				
Simulation process					
Ensemble	**Settings**				**Purpose**
NVT	Time step (fs)	0.5	Runtime (ns)	0.15	Relax structure
	Temperature (K)	300	Thermostat	Nose-Hoover	
NVE	Time step (fs)	0.5	Runtime (ns)	0.25	Relax structure
NVE	Time step (fs)	0.5	Runtime (ns)	0.1	Raise temperature
	Temperature (K)	300-1500	Thermostat	Langevin	
NVE	Time step (fs)	0.5	Runtime (ns)	1.5	Data process
	Temperature (K)	1500	Thermostat	Langevin	

IV. Structural dependence of melting point of the silicon membrane

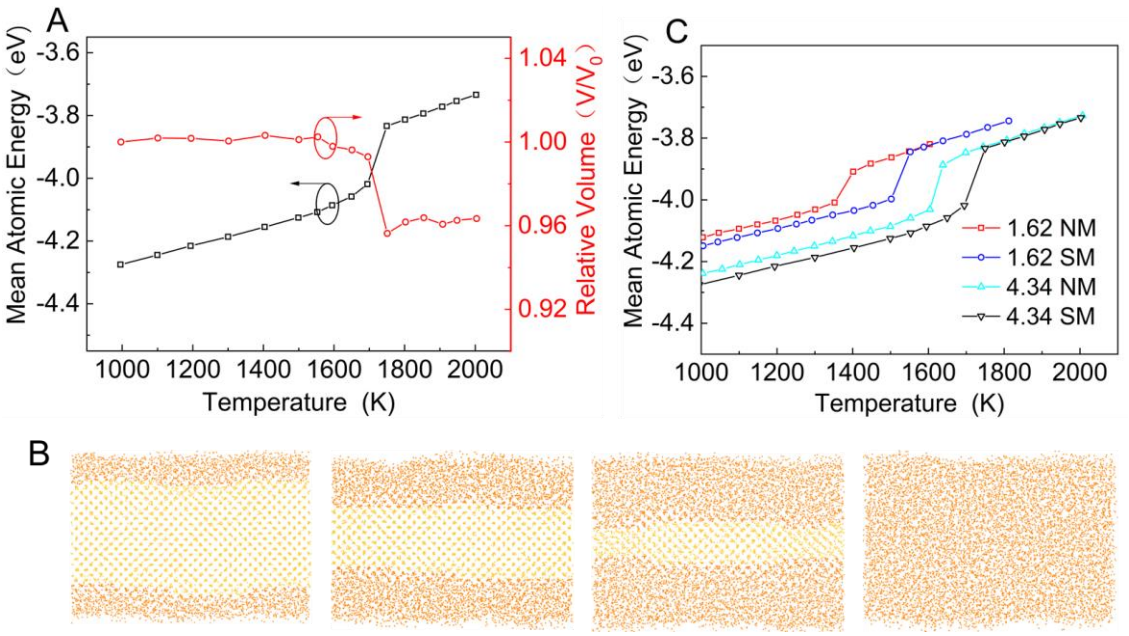

Figure S2 (A) The changes in the mean atomic energy and structural volume of 4.34 nm thick silicon solid membrane with increasing temperature. The temperature of the membrane in simulation is initially 1000 K and increases every 50 K to 2000 K. (B) Snapshots of MD simulation of the membrane in Figure S3A at 0.05, 0.2, 0.4, and 0.6 nanoseconds. The temperature is maintained around 1750 K by the Langevin thermostat. The orange area indicates that the silicon membrane has melted, whereas the yellow area retains a crystalline silicon structure. (C) Mean atomic energy versus temperature for different structures. The red, blue, cyan and black curves represent 1.62 nm thick nanoporous membrane (NM)/solid membrane (SM) and 4.34 nm thick NM/SM, respectively.

The phase change plays an important role in the subsequent deformation process and is simulated by MD. The temperature of the silicon membrane is initially 1000 K and increases every 50 K until the structure melts. The melting point of the porous membrane is essential in the simulation of deformation, which is obtained by recording the mean atomic energy and volume. As shown in Figure S2A, the total energy of atoms increases linearly with temperature, which reflects the rising process of the internal energy of silicon. The total energy of atoms increases sharply around 1750 K and then keeps increasing linearly. It can be concluded that the melting point of this structure is

around 1750 K and the structure absorbs extra energy during melting due to the latent heat of fusion [6]. From the ordinate value on the right, it can be seen that the volume of the membrane decreased by about 4% at 1750 K. Changes in volume indicates that the covalent bonds between silicon atoms and crystal structure are destroyed, resulting in volume reduction and density increase.

Figure S2B shows the melting process of the silicon membrane. Compared with atoms in the bulk of solid, surface atoms have lower cohesive energy because of weaker bond networks and fewer neighbors [7]. It can be seen that the atoms on the surface are close to each other to form new bonds at high temperatures due to the less binding than the bulk atoms. There is a surface melting layer at a temperature below the melting point. As the temperature rises, this melting layer gradually thickens and eventually leads to the melting of the silicon crystal membrane. The Lindemann criterion states that the fraction of thermal displacement atoms reaching 10% - 15% can result in the melting of the entire solid [8].

The melting point of silicon membranes shows an obvious size dependence, which is shown in Figure S2C. Membrane with a higher surface-to-volume ratio is more unstable due to extra surface energy. It is calculated that the surface-to-volume ratio of the membrane with nanopore reaches 0.79, and the value of membrane of the same thickness without nanopore is only 0.67. The higher surface-to-volume ratio results in a lower melting point due to much more defective surface atoms and higher surface energy, which can be proved by the difference in mean atomic energy as shown in Figure S2C.

V. The rounding process of the nanopore

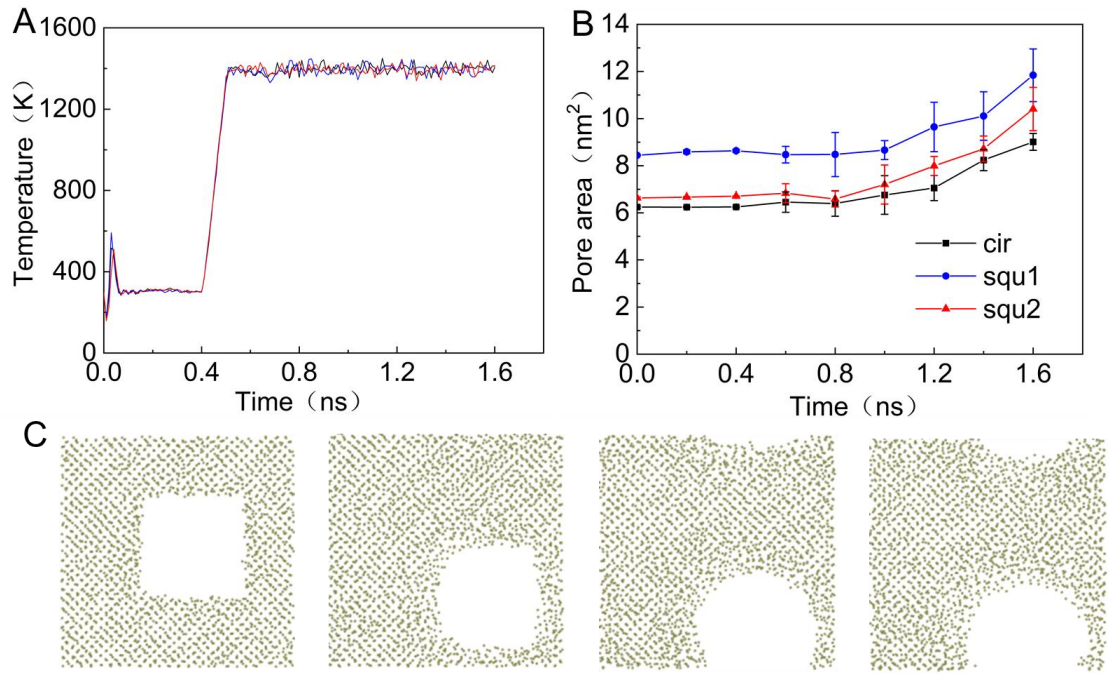

Figure S3 (A) (B) Temperature and pore area evolution for square and round pores. The black curve represents the membrane with a round nanopore, and the red and blue curves represent membranes with square pores with the Si (1 0 0) and Si (1 1 0) surface plane respectively. (C) Snapshots of MD simulation of Si (1 0 0) square nanopore at 0, 0.2, 0.4, and 0.6 nanoseconds since raising the temperature.

A curved surface under the surface tension results in a pressure difference over the interface [9]. Due to the pressure difference, the atoms along the pore edge on the surface would be pushed away from the nanopore at first. This pressure difference can also be used to explain the rounding process of a square pore in Fig S3, where the atoms in the corners will migrate to round off the edges.

Nanopores are usually non-circular before high-temperature annealing due to the highly anisotropic nature of the wet etch in silicon membranes[10]. As shown in Figure S3B, both round and square pores have the same expansion trend. It can be concluded that the geometry of pores does not affect expansion or shrinking trends. From the images in different stages shown in Figure S3C, it can be observed that the corners of square pores quickly round off since raising the temperature.

The rounding process can be explained by considering local forces generated by

surface tension. The curved surface under tension leads to pressure difference. Atoms in the corners will move under the greatest force due to the strongest curvatures. For round pores, the force is directed away from the axis of the pore. The pore area has little change since the internal atomic arrangement remains the original crystal structure. Over time, the number of thermally displaced atoms gradually increases, which leads to the entire crystal structure melting. After 1.0 ns, pores of all three shapes will expand under surface tension directed away from the axis of the pores. Therefore, high-temperature annealing can not only accurately control the size of nanopores, but also round the original irregularly shaped nanopores.

VI. The original data for nanoporous membranes

Table S2 The original data for nanoporous membranes in experiments and simulations.

Exp.	V^*	p (nm)	V (10^6 nm^3)	h (nm)	r (nm)	F (10^6 eV)
1	0.11	600	22.02	70.0	120.9	4.48
				97.7	207.2	3.84
2	0.14	400	8.94	70.0	101.4	1.97
				143.1	176.2	1.81
3	0.28	200	2.20	70.0	52.2	0.56
				68.7	50.4	0.56
4	0.33	150	1.10	70.0	46.7	0.34
				48.9	0	0.30
5	0.42	400	26.4	220.0	112.6	2.58
				187.8	78.6	2.46

Simu.	V^*	p (nm)	V (nm^3)	h (nm)	r (nm)	F (eV)
1	0.21	6.52	58.93	1.63	1.41	569.96
				2.12	2.16	553.66
				2.17	1.34	599.43

2	0.28	6.52	79.93	2.60	1.94	604.08
3	0.31	6.52	86.64	2.72	1.84	618.77
				2.63	1.75	616.32
4	0.35	6.52	98.53	2.72	1.40	628.51
				2.32	0	557.26
5	0.57	6.52	159.60	4.34	1.35	719.75
				3.76	0	557.26

VII. A comparison of the validity of the CVM and CTM

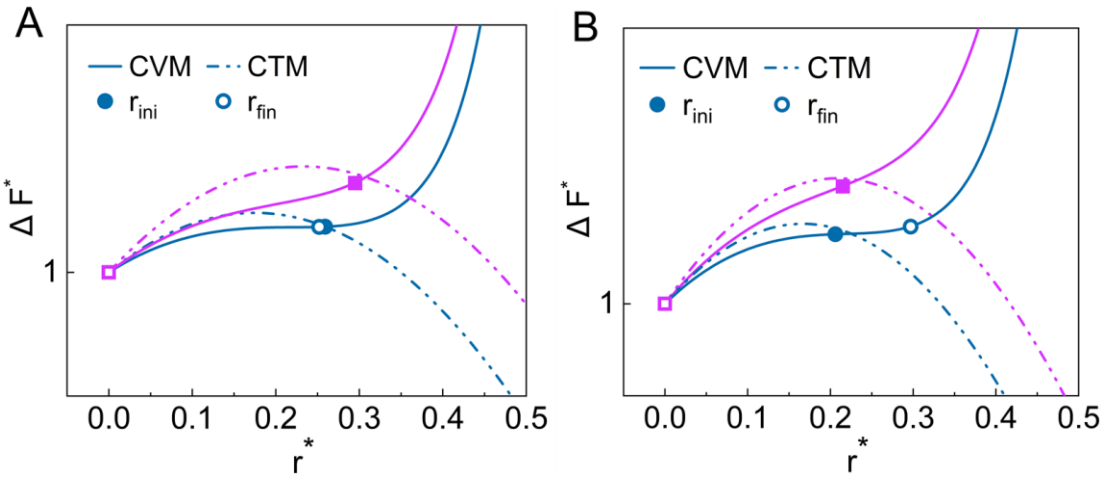

Figure S4 Experimental (A) and simulation (B) results on the evolution of nanopore size, as well as CVM and CTM model predictions.

VIII. The characteristic length for soft silicon

Generally, the shape of soft materials is determined by both the surface tension and gravity. For the sake of argument, a cube with sides d is used to discuss the effects of both. When deformation is driven by surface tension, the average strain of the cube (α) is on the order of[11]

$$\alpha = \frac{\gamma}{\mu d} \tag{S2}$$

where γ is the surface tension and μ is the small strain shear modulus. And the average strain of the cube due to gravity (β) is on the order of

$$\beta = \frac{\rho g d}{\mu} \tag{S3}$$

where ρ is the mass density and g is the acceleration of gravity.

The dominant forces that drive the deformation can be determined by comparing the magnitude of the two dimensionless strain parameters α and β. When $\alpha \gg \beta$, the effect of gravity is negligible and surface tension is dominant. For the value of α/β is 10^3, it is equal to

$$\frac{\gamma}{\rho g {d_c}^2} = 10^3 \tag{S4}$$

For soft silicon, γ is 0.733 N/m, ρ is 2.42×10^3 kg/m3 and g is 9.8 N/kg. The characteristic length (d_c) is on the order of 100 μm obtained by Eq. (S4). The surface tension is dominant for both experiments and simulations, because both their size are much smaller than 100 μm. Both the simulations and the measured results can validate the predicted trend by the constant volume model, i.e., expansion or contraction of nanopores for different starting diameters (Fig. 4).

References

[1] L. de Sousa Oliveira, N. Neophytou, Large-scale molecular dynamics investigation of geometrical features in nanoporous Si, Physical Review B, 100(3) (2019).

[2] A.J. McGaughey, M. Kaviany, Phonon transport in molecular dynamics simulations: formulation and thermal conductivity prediction, Advances in Heat Transfer, 39 (2006) 169-255.

[3] S. Plimpton, Fast parallel algorithms for short-range molecular dynamics, Journal of Computational Physics, 117(1) (1995) 1-19.

[4] G.P.P. Pun, Y. Mishin, Optimized interatomic potential for silicon and its application to thermal stability of silicene, Physical Review B, 95(22) (2017) 224103.

[5] W.C. Swope, H.C. Andersen, P.H. Berens, K.R. Wilson, A computer simulation method for the calculation of equilibrium constants for the formation of physical clusters of molecules: Application to small water clusters, The Journal of Chemical Physics, 76(1) (1982) 637-649.

[6] K.C. Fang, C.I. Weng, An investigation into the melting of silicon nanoclusters using molecular dynamics simulations, Nanotechnology, 16(2) (2005) 250-256.

[7] I.V. Talyzin, M.V. Samsonov, V.M. Samsonov, M.Y. Pushkar, V.V. Dronnikov, Size Dependence of the Melting Point of Silicon Nanoparticles: Molecular Dynamics and Thermodynamic Simulation, Semiconductors, 53(7) (2019) 947-953.

[8] F. Lindemann, The calculation of molecular vibration frequency, Z. phys, 11 (1910) 609-612.

[9] A.J. Storm, J.H. Chen, X.S. Ling, H.W. Zandbergen, C. Dekker, Electron-beam-induced deformations of SiO_2 nanostructures, Journal of Applied Physics, 98(1) (2005) 014307.

[10] C. Jian, D. Tao, L. Zewen, S. Haizhi, Controllable shrinking of silicon oxide nanopores by high temperature annealing, in: 2017 China Semiconductor Technology International Conference (CSTIC), 12-13 March 2017, IEEE, Piscataway, NJ, USA, 2017, pp. 3 pp.

[11] X. Xu, A. Jagota, S. Peng, D. Luo, M. Wu, C. Hui, Gravity and surface tension

effects on the shape change of soft materials, Langmuir, 29(27) (2013) 8665-8674.